

HybridFlow: Resource-Adaptive Subtask Routing for Efficient Edge-Cloud LLM Inference

Jiangwen Dong¹ Jiayu Li² Tianhang Zheng³ Wanyu Lin^{1,2}

Abstract

Edge-cloud collaborative inference is becoming a practical necessity for LLM-powered edge devices: on-device models often cannot afford the required reasoning capability, while cloud-only inference could be prohibitively costly and slow under strict latency and token/API budgets. However, existing edge-cloud collaboration methods often route per query or fixed steps simply based on the estimated difficulty. Such coarse and static heuristics overlook subtask dependencies, missing opportunities for parallel execution and budget-adaptive routing. To this end, we propose **HybridFlow**, a resource-adaptive edge-cloud inference framework that (i) builds a dependency-aware DAG for each query and executes newly unlocked subtasks in parallel, reducing end-to-end latency; (ii) routes each subtask online to the edge or cloud via a learned benefit-cost utility model that dynamically trades accuracy gains against token/API and latency budgets, thereby reducing unnecessary cloud usage while preserving reasoning quality. Across GPQA, MMLU-Pro, AIME24, and LiveBench-Reasoning, HybridFlow improves the cost-accuracy trade-off, reducing latency and cloud API usage while maintaining competitive accuracy against strong structured reasoning baselines. *Code: HybridFlow*

1. Introduction

Large language models (LLMs) have recently demonstrated remarkable capabilities across a wide range of tasks, especially those requiring multi-step reasoning, complex decision-making, and problem solving (Guo et al., 2025;

¹Department of Data Science and Artificial Intelligence, The Hong Kong Polytechnic University, Hong Kong SAR, China

²Department of Computing, The Hong Kong Polytechnic University, Hong Kong SAR, China ³State Key Lab. of Blockchain and Data Security, Zhejiang University, China. Correspondence to: Wanyu Lin <wan-yu.lin@polyu.edu.hk>.

Preprint. January 28, 2026.

Lin et al., 2025; Xiong et al., 2024; Yu et al., 2025). Yet, these gains come with substantial practical costs: high inference latency, large memory footprints, and non-trivial API expenses when served from the cloud (Yuan et al., 2025; Jiang et al., 2025). Such costs are particularly prohibitive for latency-sensitive and resource-constrained edge devices, where the goal is to achieve *acceptable accuracy under strict latency and cost budgets*, rather than maximizing accuracy in isolation (Ye et al., 2025; Tian et al., 2025).

A natural alternative is to deploy small models (SMs) on-device, benefiting from lightweight designs such as quantization and distillation (Wang et al., 2024a; Qu et al., 2025). However, SM-only solutions often struggle on tasks that demand deep reasoning or broad knowledge due to limited model capacity. On the other hand, cloud-only LLM inference often conflicts with practical deployment constraints, particularly *token/API cost budgets*; end-to-end latency can also become prohibitive under unfavorable network or service conditions. This tension motivates *edge-cloud collaboration*, where an on-device SM collaborates with a cloud LLM to balance accuracy, latency, and cost (Yuan et al., 2025; Akhauri et al., 2025).

Despite its promise, existing edge-cloud collaboration methods typically make *coarse-grained* decisions—e.g., routing at the query level or at a fixed reasoning-step granularity—based mainly on predicted task difficulty (Ding et al., 2024; Shao et al., 2025; Chen et al., 2024). Two limitations follow. First, coarse routing may miss opportunities for *fine-grained parallelism*: many complex queries naturally decompose into interdependent parts, where unlocked parts could be executed concurrently, but coarse allocation forces largely sequential execution. Second, practical deployments face *time-varying budgets and conditions* (e.g., fluctuating network latency, dynamic API budgets, and varying edge load), while prior approaches often use static heuristics or fixed thresholds that do not adapt online. These gaps raise the following question: *How can we design an edge-cloud framework that performs adaptive, budget-aware scheduling and routing at a fine granularity, enabling fast and token-efficient inference on complex reasoning tasks?*

We propose *HybridFlow*, a utility-driven edge-cloud inference framework that performs *subtask-level, dependency-*

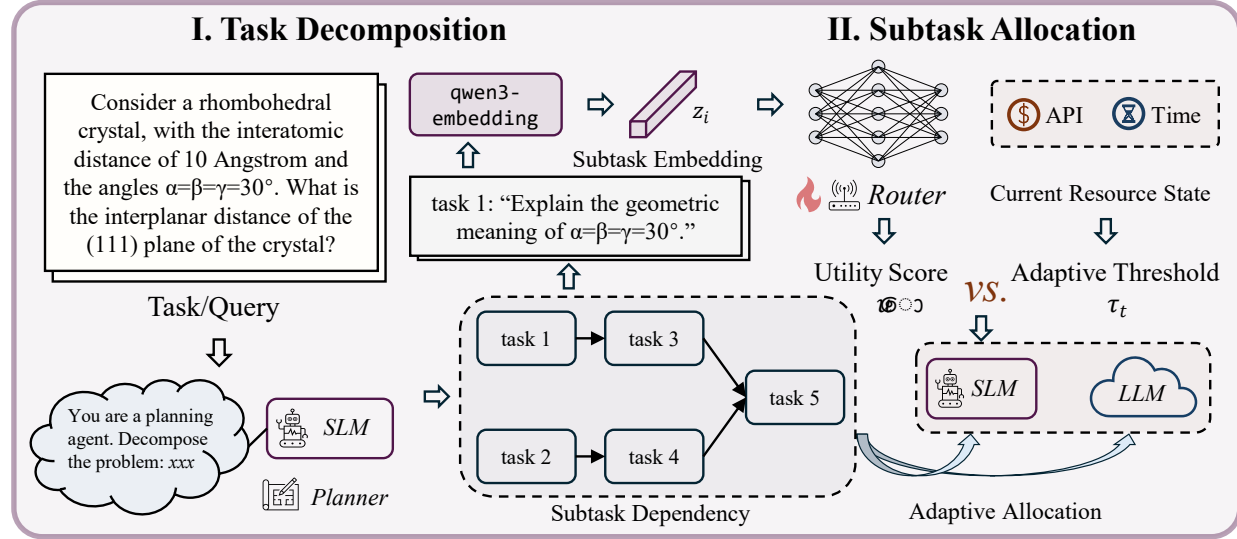


Figure 1. Overview of the **HybridFlow** framework. (I) **Task Decomposition**: The planner decomposes a complex query into a directed acyclic graph of subtasks with explicit dependencies. (II) **Subtask Allocation**: The router encodes each subtask with semantic and resource features, predicts its utility score considering quality, latency, and API cost, and adaptively allocates it to either the edge SLM or the cloud LLM for efficient collaboration.

aware collaboration. HybridFlow first decomposes a complex query into a set of subtasks with explicit dependencies, represented as a directed acyclic graph (DAG). Then, as dependencies are resolved, HybridFlow schedules newly unlocked subtasks and routes each subtask online to either the edge SM or the cloud LLM using a learned benefit–cost utility predictor, combined with an adaptive budget-aware decision rule. This design explicitly couples (i) *dependency-aware decomposition*, (ii) *parallel scheduling*, and (iii) *online budget-aware routing*, which allows HybridFlow to reduce end-to-end latency and cloud token usage under tight resource constraints.

In summary, our contributions are:

- **Fine-grained, dependency-aware edge–cloud inference.** We introduce **HybridFlow**, a subtask-level edge–cloud framework that represents complex reasoning as a DAG and executes subtasks in a dependency-triggered manner to expose parallelism beyond query-level routing.
- **Online budget-aware routing with utility modeling.** We develop a resource-aware routing mechanism that uses a learned benefit–cost utility model and an adaptive decision rule to allocate each subtask to edge or cloud under latency and API/token budgets.
- **Empirical evidence on challenging reasoning benchmarks.** We evaluate HybridFlow on four challenging benchmarks (GPQA, AIME24, LiveBench-Reasoning, and MMLU-Pro), showing improved latency–cost

trade-offs while maintaining competitive accuracy against strong structured reasoning baselines.

2. Related Work

Decomposed and Dependency-Aware Reasoning. A growing body of research aims to improve LLM reasoning efficiency by decomposing inference into smaller, more manageable units. CoT prompting (Wei et al., 2022) enhances reasoning accuracy but often increases token and latency costs due to long intermediate chains. More recent works have introduced structured decomposition and partial parallelism to address these issues. For example, SoT (Ning et al., 2024) and PASTA (Jin et al., 2025) elicit intermediate sub-questions or steps that can be executed concurrently, optimizing both accuracy and efficiency. In contrast to linear decompositions, ToT (Yao et al., 2023) organizes reasoning into a tree structure, allowing deliberate search over candidate thoughts, while GoT (Besta et al., 2024) and S-DAG (Dong et al., 2025) extend this idea to graph-based reasoning, enabling flexible, reusable intermediate nodes with complex dependency patterns.

Budgeted Edge–Cloud Routing and Online Adaptation. Edge–cloud collaboration often involves routing mechanisms where simpler models handle easier tasks and offload more complex ones to stronger models, or where tasks are decomposed and distributed across multiple models (Wang et al., 2025; Li et al., 2025; Ding et al., 2024; Shao et al., 2025). However, many systems operate at coarse granularity (e.g., query-level or stage-level) and do not explicitly opti-

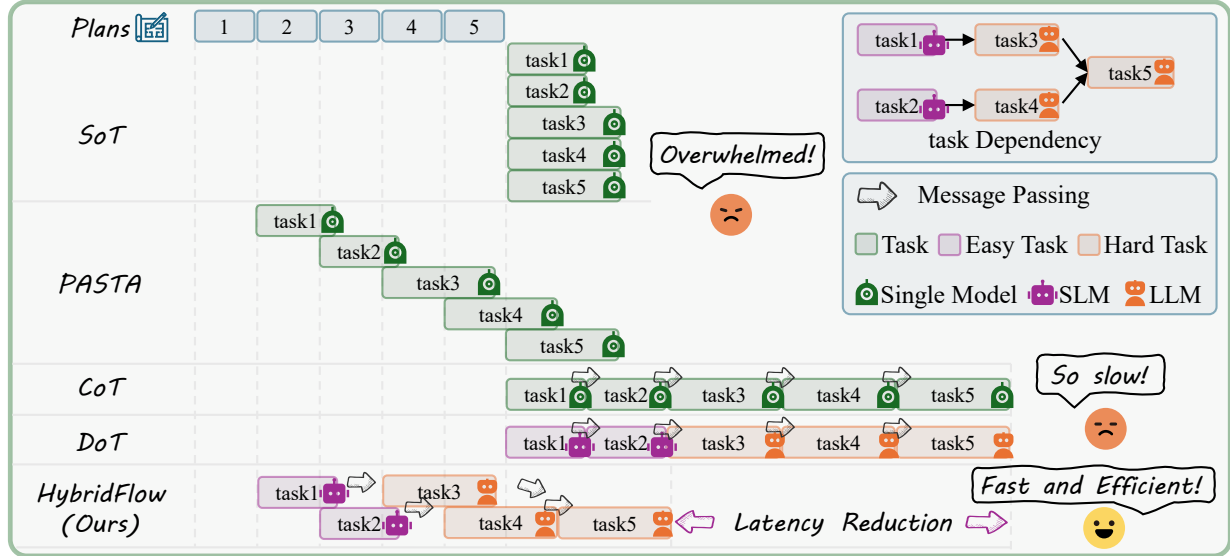


Figure 2. Overview of comparative LLM inference pipeline. **HybridFlow** uniquely integrates dependency-aware planning concurrently with parallel execution. This achieves an optimal balance between speed and reasoning quality by actively exploiting concurrent opportunities within a logically constrained workflow.

mize for tight, multi-resource constraints such as latency and API budgets. Cost-aware routing methods, like LLM cascades using mixture-of-thought representations (Yue et al., 2023) and FrugalGPT (Chen et al., 2023), address budget-quality trade-offs by selectively invoking stronger models at various stages. Related work like SplitReason (Akhauri et al., 2025) also explores fine-grained offloading, learning to delegate specific reasoning steps to stronger models. However, many of these learned routers rely on stationary assumptions or fixed thresholds, which can hinder performance when the workload, network conditions, or pricing fluctuate. In contrast, HybridFlow adapts dynamically to these changes, optimizing edge-cloud allocation in real-time for more robust and efficient reasoning.

3. HybridFlow Framework

HybridFlow enables efficient edge–cloud collaborative inference by combining dependency-aware task planning with cost-aware routing. As illustrated in Fig. 1, the system has two tightly connected components. First, an edge-side planner decomposes a complex query into a set of interdependent subtasks and constructs a task-level DAG, enabling each subtask to execute as soon as its prerequisites are resolved. This exposes fine-grained parallelism and reduces wall-clock latency compared with strictly sequential reasoning. Second, a resource-aware router assigns each subtask to either the edge model M_{edge} or the cloud LLM M_{cloud} based on its predicted utility and the system’s real-time budget status. By coupling decomposition with budget-constrained routing, HybridFlow explicitly balances accuracy and efficiency.

We summarize the notations in Table 4 and outline the full procedure in Algorithm 1.

3.1. Preliminaries

We consider an edge–cloud inference setting in which a small edge model M_{edge} collaborates with a large cloud model M_{cloud} to solve a query Q . The query is decomposed into n subtasks $\{t_1, \dots, t_n\}$, each executable either on M_{edge} or on M_{cloud} . The routing decision for each subtask must trade off the accuracy benefit of using the cloud against its resource cost.

For each subtask t_i , we define:

- Δq_i : expected *accuracy gain* of executing t_i on the cloud instead of the edge;
- Δl_i : additional *latency cost* (in seconds) incurred by cloud execution;
- Δk_i : additional *API usage cost* (in tokens or price units) incurred by cloud execution.

In practice, Δq_i is estimated offline using automatic metrics such as BartScore (Yuan et al., 2021) by comparing cloud and edge outputs against references or high-quality pseudo-labels. This profiling is done once and does not affect online latency.

To place latency and API usage on a common scale, we define a normalized offloading cost.

Definition 3.1 (Normalized Cost). For each subtask t_i , the

Algorithm 1 HybridFlow: Dependency-Aware Scheduling with Budget-Adaptive Routing

Input: Query Q ; edge model M_{edge} ; cloud model M_{cloud} ; planner M_P ; budgets C_{\max} ; router f_θ ; step size η ; threshold params (τ_0, γ)

Output: Final response R

Stage 1: Decompose and initialize

$(T, E) \leftarrow \text{Decompose}(Q; M_P)$; build DAG $G = (T, E)$
 Initialize in-degrees $\text{deg}(\cdot)$ on G ; answers map $A[\cdot] \leftarrow \emptyset$
 Initialize ready queue $\mathcal{F} \leftarrow \{t \in T : \text{deg}(t) = 0\}$
 Initialize cumulative cost $C_{\text{used}} \leftarrow 0$ and dual variable $\lambda \leftarrow 0$

Stage 2: Schedule, route, and execute

while \mathcal{F} not empty **do**
 Pop a ready subtask t from \mathcal{F}
 $x \leftarrow (t, \{A[p]\}_{p \in \text{Dep}(t)})$
 $\hat{u} \leftarrow \sigma(f_\theta(\text{Embed}(t)))$; // offline utility estimate
 $\bar{u} \leftarrow \text{Calibrate}(\hat{u}, \text{online signals})$
 $\lambda \leftarrow [\lambda + \eta(C_{\text{used}} - C_{\max})]_+$; // Eq. (10)
 $\tau \leftarrow \text{clip}(\tau_0 + \gamma\lambda, 0, 1)$; // Eq. (11)
if $\bar{u} > \tau$ **and** $C_{\text{used}} + c(t) \leq C_{\max}$ **then**
 | $A[t] \leftarrow M_{\text{cloud}}(x)$; $C_{\text{used}} \leftarrow C_{\text{used}} + c(t)$
else
 | $A[t] \leftarrow M_{\text{edge}}(x)$
foreach $s \in \text{Succ}(t)$ **do**
 | $\text{deg}(s) \leftarrow \text{deg}(s) - 1$; **if** $\text{deg}(s) = 0$ **then**
 | | $\text{push } s \text{ into } \mathcal{F}$

Stage 3: Aggregate

$R \leftarrow \text{Aggregate}(\{A[t]\}_{t \in T} \text{ in topological order})$
return R

normalized cost of offloading is

$$c_i = \text{clip}\left(\left(\frac{\Delta l_i}{l_{\max}^{\text{sub}}} + \frac{\Delta k_i}{k_{\max}^{\text{sub}}}\right)/2, 0, 1\right) \in [0, 1], \quad (1)$$

where l_{\max}^{sub} and k_{\max}^{sub} are per-subtask upper bounds on additional latency and API cost. Typically $\Delta l_i \leq l_{\max}^{\text{sub}}$ and $\Delta k_i \leq k_{\max}^{\text{sub}}$, so c_i is bounded and comparable across subtasks.

We use a binary variable $r_i \in \{0, 1\}$ to indicate whether t_i is offloaded to the cloud ($r_i = 1$) or executed on the edge ($r_i = 0$). Intuitively, subtasks with larger Δq_i and smaller c_i are more attractive to offload.

Definition 3.2 (Utility). The *utility* of offloading subtask t_i is the normalized benefit–cost ratio

$$u_i = \text{clip}\left(\frac{\Delta q_i}{c_i + \varepsilon}, 0, 1\right), \quad (2)$$

where $\varepsilon > 0$ is a small constant (e.g., 10^{-4}) for numerical stability and $\text{clip}(\cdot, 0, 1)$ truncates the value to $[0, 1]$. Con-

ceptually, u_i measures the accuracy improvement per unit normalized cost and serves as the ideal offloading score.

Knapsack Formulation. Using these quantities, subtask allocation can be written as a resource-constrained optimization problem. Let $\mathbf{r} = (r_1, \dots, r_n)$ denote the allocation vector. We seek to maximize the total accuracy gain under a normalized resource budget:

$$\max_{\mathbf{r} \in \{0,1\}^n} \sum_{i=1}^n r_i \Delta q_i \quad \text{s.t.} \quad \sum_{i=1}^n r_i c_i \leq C_{\max}, \quad (3)$$

where C_{\max} is the total normalized budget per query. This is exactly a 0–1 knapsack problem: each subtask is an item with value Δq_i and weight c_i under capacity C_{\max} .

Lagrangian Relaxation and Threshold Structure. Introducing a Lagrange multiplier $\lambda \geq 0$ for the budget constraint, the Lagrangian is

$$\mathcal{L}(\mathbf{r}, \lambda) = \sum_{i=1}^n r_i \Delta q_i - \lambda \left(\sum_{i=1}^n r_i c_i - C_{\max} \right) \quad (4)$$

$$= \lambda C_{\max} + \sum_{i=1}^n r_i (\Delta q_i - \lambda c_i). \quad (5)$$

For fixed λ , the relaxed problem decouples across subtasks, and the optimal decision follows a threshold rule:

$$r_i^*(\lambda) = \mathbb{I}[\Delta q_i - \lambda c_i > 0] = \mathbb{I}\left[\frac{\Delta q_i}{c_i} > \lambda\right]. \quad (6)$$

Thus, an ideal policy offloads subtasks with sufficiently large benefit–cost ratio. This structure motivates HybridFlow learned utility and online thresholding in Sec. 3.3.

3.2. Task Decomposition and Execution Pipeline

Effective task decomposition forms the backbone of HybridFlow, as it determines both the logical structure and the degree of parallelism in the inference pipeline. Given a query Q , the planner must identify meaningful subtasks and their dependencies so that reasoning remains coherent while supporting concurrent execution on edge and cloud workers. As illustrated in Fig. 2, existing frameworks typically sit at two extremes: approaches such as SoT (Ning et al., 2024) and PASTA (Jin et al., 2025) aggressively parallelize steps with limited regard for dependencies, while CoT (Wei et al., 2022) and DoT (Shao et al., 2025) enforce strictly sequential execution, preserving correctness but incurring high latency.

HybridFlow sidesteps this dilemma by explicitly modeling dependencies while still exploiting available parallelism. We leverage an edge-deployed planner M_P and elicit its behavior with an Explain–Analyze–Generate (EAG) metaprompt (Gu et al., 2025). The prompt guides M_P through

three stages: (i) identifying key elements of the query, (ii) analyzing and breaking the query into interrelated subtasks, and (iii) generating a structured representation of the overall solution plan. To make this process robust, we curate high-quality exemplars by evaluating multiple models on 100 queries from s1k (Muennighoff et al., 2025) and selecting examples that exhibit strong logical grounding, clear dependency structure, and non-trivial parallelism. These exemplars are used as few-shot demonstrations for planner.

Formally, we write the decomposition process as

$$(T, E) = \text{Decompose}(Q; M_P), \quad (7)$$

where $T = \{t_1, \dots, t_n\}$ is the set of subtasks and $E \subseteq T \times T$ encodes directed prerequisite relations. In practice, M_P outputs an XML-formatted plan whose parent fields are parsed into a task-level DAG $G(Q) = (T, E)$. A scheduler maintains a queue of *ready* subtasks whose parents have completed and dispatches them immediately to either M_{edge} or M_{cloud} according to the routing policy in Sec. 3.3. This design preserves explicit dependencies while allowing independent subtasks to proceed in parallel, reducing end-to-end latency compared with purely sequential execution. See prompts in Figure 6.

3.3. Utility-based Subtask Routing

The router decides whether to assign a subtask to M_{cloud} by estimating the utility of offloading to the cloud. It serves as a lightweight approximation to the knapsack allocation in Eq. (3), while adapting its conservativeness online according to real-time budget usage.

Offline Utility Estimation. Each subtask t_i is encoded into a semantic embedding z_i using the qwen3-embedding-0.6b model (Zhang et al., 2025). A multilayer perceptron (MLP) computes a normalized estimated utility

$$\hat{u}_i = \sigma(f_\theta(z_i)) \in (0, 1), \quad (8)$$

where σ is the sigmoid function. The estimate \hat{u}_i is trained to approximate the ideal utility u_i in Def. 3.2.

Router Training. Supervision is derived by profiling subtasks on both edge and cloud models. The observed accuracy gain Δq_i and normalized cost c_i define the utility target u_i via Eq. (2). The router is trained with MSE:

$$\mathcal{L}(\theta) = \frac{1}{N} \sum_{i=1}^N (\hat{u}_i - u_i)^2. \quad (9)$$

This amortizes offline profiling into a fast online decision and provides a strong warm-start.

Online Dual Thresholding. During inference, subtasks become available online as dependencies resolve. Motivated by the threshold structure in Eq. (6), HybridFlow maintains a dual variable $\lambda_t \geq 0$ as a shadow price for normalized resource consumption and updates it via a projected subgradient step:

$$\lambda_{t+1} = \left[\lambda_t + \eta(C_{\text{used}}(t) - C_{\text{max}}) \right]_+, \quad (10)$$

where $\eta > 0$ is a step size and $C_{\text{used}}(t) = \sum_{j \leq t} r_j c_j$ is the cumulative normalized cost used so far. When the system overspends, λ_t increases and the routing policy becomes more conservative.

We map the shadow price to a normalized routing threshold $\tau_t \in [0, 1]$ via a monotone transform:

$$\tau_t = \text{clip}(\tau_0 + \gamma \lambda_t, 0, 1), \quad (11)$$

where τ_0 is a base threshold and γ controls sensitivity. The router then offloads t_i if its (possibly calibrated) utility exceeds τ_t :

$$r_i = \mathbb{I}[\bar{u}_i > \tau_t], \quad \bar{u}_i = \begin{cases} \tilde{u}_i, & \text{if online calibration,} \\ \hat{u}_i, & \text{otherwise.} \end{cases} \quad (12)$$

This rule approximates the relaxed Lagrangian policy in Eq. (6) while adapting to real-time budget consumption.

Contextual Bandit Calibration. Offline utilities \hat{u}_i may be miscalibrated under system shifts (e.g., cloud latency changes) or task shifts (e.g., different query domains). To adapt online with partial feedback, we introduce a lightweight calibration head that refines \hat{u}_i using runtime context. Let s_i denote a feature vector of online signals, such as remaining budget and planner-provided attributes. We define a calibrated utility:

$$\tilde{u}_i = \text{clip}(\alpha \hat{u}_i + \beta + w^\top s_i, 0, 1), \quad (13)$$

where (α, β, w) are updated online.

HybridFlow only observes the quality gain Δq_i when t_i is offloaded ($r_i = 1$), yielding a contextual bandit setting with partial feedback. We define a cost-aware reward consistent with the Lagrangian form:

$$R_i = \Delta q_i - \lambda_t c_i, \quad (14)$$

and update (α, β, w) online using a standard contextual bandit strategy (e.g., LinUCB) to ensure exploration. This calibration is lightweight and can be enabled when robustness to shifts is desired.

Table 1. Accuracy (%), mean \pm std of HybridFlow and baseline methods across four benchmarks. **Bold** denotes the highest accuracy and underline indicates the second-highest. Direct Prompt results (shaded) are reference single-model baselines and are excluded from ranking. HybridFlow achieves competitive accuracy while operating under edge–cloud collaboration constraints.

Method	Model	GPQA	MMLU-Pro	AIME24	LiveBench-Reasoning	Avg. (\uparrow)
Direct Prompt	L3B	16.89 \pm 1.05	22.83 \pm 1.31	4.44 \pm 1.57	12 \pm 2.86	14.04
Direct Prompt	G4.1	51.79 \pm 1.17	<u>65.5</u> \pm 1.47	37.78 \pm 1.57	<u>58.25</u> \pm 0.75	53.33
CoT (Wei et al., 2022)	L3B	25.54 \pm 1.57	31.67 \pm 0.85	<u>5.56</u> \pm 1.57	15.6 \pm 1.93	19.59
CoT	G4.1	57.28 \pm 0.73	72 \pm 0.71	44.42 \pm 1.59	62.25 \pm 0.75	58.99
SoT (Ning et al., 2024)	L3B	30.24 \pm 0.34	31.67 \pm 2.87	1.11 \pm 1.57	17.33 \pm 1.89	20.09
SoT	G4.1	<u>56.4</u> \pm 0.99	71.8 \pm 1.03	28.89 \pm 1.57	54.5 \pm 1.08	52.90
PASTA (Jin et al., 2025)	L3B	28.67 \pm 2.83	25.84 \pm 2.65	2.22 \pm 1.92	14.75 \pm 1.02	17.87
PASTA	G4.1	41.28 \pm 2.87	75.52 \pm 1.77	32.1 \pm 1.57	33.33 \pm 1.62	45.56
HybridLLM (Ding et al., 2024)	L3B&G4.1	52.9 \pm 0.94	43 \pm 0.82	22.22 \pm 1.57	36.67 \pm 0.62	38.70
DoT (Shao et al., 2025)	L3B&G4.1	50.54 \pm 3.04	66 \pm 1.63	21.11 \pm 3.14	48.33 \pm 1.89	46.50
HybridFlow (Ours)	L3B&G4.1	53.33 \pm 2.03	72.54 \pm 0.65	<u>36.67</u> \pm 1.57	<u>58.83</u> \pm 1.48	<u>55.34</u>

4. Experiments

4.1. Experiment Setup

Datasets and Metrics. We evaluate *HybridFlow* on four reasoning benchmarks spanning mathematical, scientific, and general domains: *GPQA* (Rein et al., 2024); *AIME24*; *MMLU-Pro* (Wang et al., 2024b), and *LiveBench-Reasoning* (White et al., 2025). We select three metrics that jointly capture reasoning quality and system efficiency. (i) Acc measures the correctness of reasoning by comparing model outputs with gold answers across all benchmarks. (ii) C_{time} denotes the end-to-end inference latency per query, including decomposition, routing, and execution. (iii) C_{API} quantifies the number of tokens consumed by cloud LLM calls, reflecting token efficiency and cost.

Baselines. We compare *HybridFlow* with representative task decomposition methods from single-model and edge–cloud collaborative paradigms, as well as a direct prompting baseline. For single-model methods, we select *CoT* (Wei et al., 2022), *SoT* (Ning et al., 2024) and *PASTA* (Jin et al., 2025). For collaborative inference, we select *HybridLLM* (Ding et al., 2024), and *DoT* (Shao et al., 2025).

Implementation Details. HybridFlow deploys Llama3.2-3B on the edge device in two roles: (i) as the *planner* M_P that decomposes each query into a task-level DAG, and (ii) as the *edge executor* M_{edge} that runs subtasks not offloaded. Each subtask is encoded with qwen3-embedding-0.6b into an embedding z_i , which is fed to a lightweight router: a two-hidden-layer MLP that predicts an offline utility estimate \hat{u}_i . The router is *offline warm-started* with AdamW (learning rate 1×10^{-4}) by regressing to profiled utility targets. During inference, HybridFlow performs *online adaptation* with dual-threshold updates that track budget consumption; an online calibration head is updated from partial feedback

via a contextual-bandit strategy. Routing decisions use the current threshold to assign each ready subtask to either M_{edge} or the cloud model M_{cloud} (GPT-4.1, via API). All edge-side computation (planning, local execution, and embedding) runs on a single NVIDIA RTX 3090 GPU (24GB). All LLM use a fixed temperature of 0.6.

4.2. Results

Task decomposition enhances multi-step reasoning performance. Across all benchmarks, methods that explicitly decompose tasks into structured intermediate steps show clear advantages over direct prompting. As shown in Table 1, CoT with GPT-4.1 attains the highest overall accuracy among non-Prompt methods (**58.99%**), confirming the strong benefits of stepwise reasoning. HybridFlow closely follows with an average accuracy of 55.34%, outperforming SoT and PASTA variants while remaining competitive with the strongest single-model reasoning approach. This demonstrates that HybridFlow’s planner produces decomposition structures not only logically aligned with the tasks but also highly executable by collaborating edge and cloud models.

Parallel execution substantially reduces end-to-end latency. HybridFlow’s dependency-aware DAG planning enables fine-grained concurrency during subtask execution. This design significantly reduces wall-clock latency compared to sequential or coarse-grained hybrid pipelines. As reported in Table 2, HybridFlow achieves an average C_{time} of 17.48 s, outperforming HybridLLM (24.45 s) by a large margin and even improving over the sequentially constrained DoT baseline (18.32 s). These results confirm that exploiting parallelism within logically valid execution windows can effectively offset the overhead of multi-step reasoning, leading to faster and more responsive inference.

Table 2. Efficiency comparison of HybridFlow and baselines on four reasoning benchmarks. Lower values indicate better efficiency for both end-to-end inference time (C_{time} , in seconds) and cloud API cost (C_{API}). Bold denotes the best and underline marks the second-best performance among edge–cloud collaboration baselines. Direct Prompt rows (shaded) serve as reference points and are excluded from ranking. HybridFlow consistently improves latency and cloud usage through dependency-aware parallel execution and adaptive routing.

Method	Model	Metric	GPQA	MMLU-Pro	AIME24	LiveBench-Reasoning	Avg. (\downarrow)
Direct Prompt	L3B	C_{time}	6.61 ± 0.50	7.03 ± 0.64	9.92 ± 1.51	13.34 ± 0.40	9.23
Direct Prompt	G4.1	C_{time}	15.26 ± 1.85	11.77 ± 0.18	50.44 ± 1.64	36.77 ± 1.61	28.56
Direct Prompt	L3B	C_{API}	–	–	–	–	–
Direct Prompt	G4.1	C_{API}	0.0094	0.0060	0.0256	0.0181	0.0148
CoT (Wei et al., 2022)	L3B	C_{time}	11.99 ± 0.25	10.87 ± 0.45	22.76 ± 4.78	14.00 ± 0.17	14.91
CoT	L3B	C_{API}	–	–	–	–	–
CoT	G4.1	C_{time}	18.26 ± 2.49	19.35 ± 0.22	56.70 ± 2.66	29.77 ± 0.79	31.02
CoT	G4.1	C_{API}	0.0185	0.0115	0.0445	0.0330	0.0269
SoT (Ning et al., 2024)	L3B	C_{time}	18.55 ± 0.31	10.95 ± 0.48	15.20 ± 0.85	14.61 ± 0.78	14.83
SoT	L3B	C_{API}	–	–	–	–	–
SoT	G4.1	C_{time}	16.27 ± 1.57	11.43 ± 0.03	29.52 ± 0.56	20.87 ± 0.81	19.52
SoT	G4.1	C_{API}	0.0154	0.0095	0.0328	0.0206	0.0196
PASTA (Jin et al., 2025)	L3B	C_{time}	8.77 ± 1.19	14.15 ± 0.68	12.43 ± 1.24	15.65 ± 0.58	12.75
PASTA	L3B	C_{API}	–	–	–	–	–
PASTA	G4.1	C_{time}	12.21 ± 1.72	8.76 ± 0.76	21.37 ± 1.65	19.14 ± 1.29	15.37
PASTA	G4.1	C_{API}	0.0262	0.0179	0.0474	0.0338	0.0313
HybridLLM (Ding et al., 2024)	L3B&G4.1	C_{time}	15.96 ± 1.74	14.90 ± 0.40	40.11 ± 2.25	26.82 ± 1.65	24.45
HybridLLM	L3B&G4.1	C_{API}	0.0160	0.0050	0.0168	0.0135	0.0128
DoT (Shao et al., 2025)	L3B&G4.1	C_{time}	15.79 ± 0.67	11.00 ± 0.45	29.91 ± 2.50	16.59 ± 0.80	<u>18.32</u>
DoT	L3B&G4.1	C_{API}	<u>0.0078</u>	0.0056	<u>0.0138</u>	0.0087	<u>0.009</u>
HybridFlow (Ours)	L3B&G4.1	C_{time}	15.24 ± 0.30	11.85 ± 0.38	26.40 ± 1.54	16.41 ± 0.59	17.48
HybridFlow (Ours)	L3B&G4.1	C_{API}	0.0075	<u>0.0052</u>	0.0135	<u>0.0091</u>	0.0088

HybridFlow delivers the best accuracy–efficiency trade-off. While HybridFlow’s accuracy approaches the top-performing CoT with GPT-4.1, it does so with dramatically lower token consumption and latency. Table 2 shows that HybridFlow achieves the lowest average C_{API} (**0.0088**) among all collaborative baselines, indicating high token efficiency in cloud usage. When considering both accuracy and efficiency jointly, HybridFlow consistently dominates alternative hybrid systems: it improves accuracy relative to HybridLLM and DoT while simultaneously reducing latency and API cost. This demonstrates that HybridFlow effectively balances the strengths of edge and cloud models through adaptive routing and parallelized task execution, achieving a superior overall accuracy–efficiency frontier.

4.3. Ablation Study

In this section, we conduct a series of ablation studies to validate effectiveness of our adaptive allocation mechanism. Our goal is to demonstrate that Router is crucial for achieving a balance between latency, cost, and performance.

Router for Subtask Allocation. We evaluate our **adaptive router** against deterministic and naive allocation strategies (Table 3). Using only the edge model (Edge) incurs zero

API cost but yields the lowest accuracy (25.54%), whereas executing all subtasks in the cloud (Cloud) achieves the highest accuracy (57.28%) with higher latency and API cost ($C_{\text{API}}=0.0185$). The *Random* baseline improves accuracy (46.00%) by occasionally offloading, but lacks a principled mechanism to prioritize high-value subtasks, resulting in lower utility. In contrast, *HybridFlow* attains 53.33% accuracy at a much lower API cost ($C_{\text{API}}=0.0075$) and achieves the *highest* utility score (0.7940), indicating a more favorable accuracy–cost trade-off under our unified metric. Overall, these results suggest that the learned router better aligns subtask-level benefit with resource expenditure.

Offload Ratio between Edge and Cloud. To characterize the router’s within-query allocation, we count how many subtasks are executed on the edge vs. the cloud at each subtask position. Figure 3 shows a clear position-dependent pattern rather than uniform offloading. At early positions, the adaptive threshold is relatively low and the remaining budget is large, making cloud execution more likely. As reasoning proceeds, the threshold increases and eventually saturates; correspondingly, routing shifts toward the edge, with few cloud calls at later positions. Meanwhile, the total number of subtasks decreases at deeper positions, suggesting that many queries resolve key reasoning steps early. Overall,

Table 3. Ablation of routing strategies on GPQA. We compare offload rate, accuracy, latency, API cost, normalized total cost, and utility (see Sec. 3 for definitions). HybridFlow achieves the best trade-off between accuracy and cost, the highest utility score.

Method	Offload Rate (%)	Accuracy (%)	Latency (s)	API Cost (\$)	Norm. Cost c (↓)	Utility u (↑)
Edge (<i>Llama3.2-3B</i>)	0	25.54	11.99	0	—	—
Cloud (<i>GPT-4.1</i>)	100	57.28	18.26	0.0185	0.7760	0.4090
Random (<i>Llama3.2-3B + GPT-4.1</i>)	42.1	46.00	15.15	0.0075	0.3455	0.5922
Fixed Threshold ($\tau_0 = 0.5$)	41.18	51.62	15.88	0.0088	0.4145	0.6292
HybridFlow (Ours)	40.48	53.33	15.24	0.0075	0.3500	0.7940

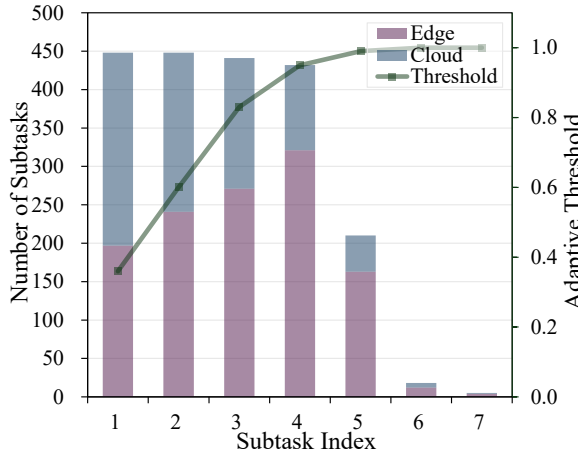


Figure 3. Distribution of executed subtasks between the edge and cloud models across subtask positions on GPQA. Bars show the number of subtasks executed on the edge (purple) and on the cloud (blue) at each subtask index, and the line shows the average adaptive threshold at that position.

HybridFlow concentrates cloud usage on early, high-impact subtasks and relies on the edge model for downstream subtasks as the routing criterion becomes stricter.

Effect of Fixed Offload Thresholds. To isolate the role of the base threshold, we vary the fixed offload threshold τ_0 in Eq. 11 *without* dynamic resource adaptation and measure accuracy, offload rate, latency, and cost. As shown in Figure 4 and Table 5, increasing τ_0 makes routing more conservative: the offload rate decreases monotonically from 100.00% ($\tau_0=0$) to 0.00% ($\tau_0=1$), and the normalized cost decreases accordingly from $c=0.7760$ to $c=0.2000$ at $\tau_0=0.9$ (and is undefined when no cloud calls are made). Accuracy declines smoothly over the same range, from 57.28% at $\tau_0=0$ to 25.54% at $\tau_0=1$. This consistent trade-off suggests that the predicted utilities $\hat{u}_i \in [0, 1]$ yield coherent decision boundaries when compared against the normalized cost scale $c_i \in [0, 1]$.

Notably, the utility score peaks at $\tau_0=0.6$ with $u=0.6329$, where the router maintains 47.85% accuracy at a moderate normalized cost ($c=0.3525$) and an offload rate of 33.51%. Moving to a looser threshold (e.g., $\tau_0=0.5$) increases both accuracy (51.62%) and cost ($c=0.4145$) but slightly reduces

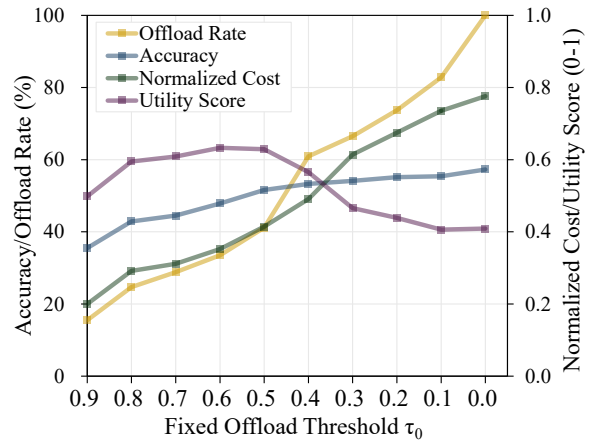


Figure 4. Performance-cost trends under different fixed offload thresholds τ_0 on the GPQA benchmark. Increasing τ_0 makes the router more conservative, leading to lower offload rate and cost but gradually reducing accuracy.

utility (0.6292), while more aggressive offloading further raises cost and eventually decreases utility (e.g., $u=0.5652$ at $\tau_0=0.4$ and $u=0.4090$ at $\tau_0=0$). These results indicate that a single global threshold has a narrow optimal operating region.

In contrast, *HybridFlow* achieves a substantially higher utility (0.7940 in Table 3) by dynamically adapting routing decisions to the evolving budget, outperforming any fixed-threshold setting while avoiding both excessive offloading and premature underutilization.

5. Conclusion

In this paper, we introduce *HybridFlow*, a resource-aware inference framework that formulates fast, token-efficient collaborative reasoning as a sequential decision process. By decomposing complex queries into a dependency-aware DAG, HybridFlow optimizes the reasoning path and facilitates parallel subtask execution. Our resource-aware subtask router, which moves beyond rigid, coarse-grained allocation, enables HybridFlow to adaptively assign subtasks to edge or cloud resources. This process allows the framework to achieve superior performance while balancing inference

time, token usage, and real-time budget states. On comprehensive evaluations including GPQA, MMLU-Pro, AIME, and LiveBench-Reasoning, HybridFlow effectively outperforms sequential and coarse-grained baselines, demonstrating significant reductions in both end-to-end latency and overall token consumption. These results demonstrate the promise of our adaptive, parallel-aware routing framework for orchestrating efficient edge-cloud AI.

References

Akhauri, Y., Fei, A., Chang, C.-C., AbouElhamayed, A. F., Li, Y., and Abdelfattah, M. S. Splitreason: Learning to offload reasoning, 2025. URL <https://arxiv.org/abs/2504.16379>.

Besta, M., Blach, N., Kubicek, A., Gerstenberger, R., Podstawska, M., Gianinazzi, L., Gajda, J., Lehmann, T., Niewiadomski, H., Nyczyk, P., et al. Graph of thoughts: Solving elaborate problems with large language models. In *Proceedings of the AAAI conference on artificial intelligence*, volume 38, pp. 17682–17690, 2024.

Chen, D., Zhuang, Y., Zhang, S., Liu, J., Dong, S., and Tang, S. Data shunt: Collaboration of small and large models for lower costs and better performance. In *Proceedings of the AAAI Conference on Artificial Intelligence*, volume 38, pp. 11249–11257, 2024.

Chen, L., Zaharia, M., and Zou, J. Frugalgpt: How to use large language models while reducing cost and improving performance. *arXiv preprint arXiv:2305.05176*, 2023.

Ding, D., Mallick, A., Wang, C., Sim, R., Mukherjee, S., Rühle, V., Lakshmanan, L. V. S., and Awadallah, A. H. Hybrid LLM: Cost-efficient and quality-aware query routing. In *The Twelfth International Conference on Learning Representations*, 2024. URL <https://openreview.net/forum?id=02f3mUtqnM>.

Dong, J., Lin, Z., Lin, W., and Zhang, M. S-dag: A subject-based directed acyclic graph for multi-agent heterogeneous reasoning. *arXiv preprint arXiv:2511.06727*, 2025.

Gu, W., Han, J., Wang, H., Li, X., and Cheng, B. Explain-analyze-generate: A sequential multi-agent collaboration method for complex reasoning. In Rambow, O., Wanner, L., Apidianaki, M., Al-Khalifa, H., Eugenio, B. D., and Schockaert, S. (eds.), *Proceedings of the 31st International Conference on Computational Linguistics*, pp. 7127–7140, Abu Dhabi, UAE, January 2025. Association for Computational Linguistics. URL <https://aclanthology.org/2025.coling-main.475/>.

Guo, M.-H., Xu, J., Zhang, Y., Song, J., Peng, H., Deng, Y.-X., Dong, X., Nakayama, K., Geng, Z., Wang, C., Ni, B., Yang, G.-W., Rao, Y., Peng, H., Hu, H., Wetzstein, G., and min Hu, S. RBench: Graduate-level multi-disciplinary benchmarks for LLM & MLLM complex reasoning evaluation. In *Forty-second International Conference on Machine Learning*, 2025.

Jiang, Y., Fu, F., Yao, X., Wang, T., Cui, B., Klimovic, A., and Yoneki, E. Thunderserve: High-performance and cost-efficient llm serving in cloud environments. *arXiv preprint arXiv:2502.09334*, 2025.

Jin, T., Cheng, E. Y., Ankner, Z., Saunshi, N., Elias, B. M., Yazdanbakhsh, A., Ragan-Kelley, J., Subramanian, S., and Carbin, M. Learning to keep a promise: Scaling language model decoding parallelism with learned asynchronous decoding. In *Forty-second International Conference on Machine Learning*, 2025. URL <https://openreview.net/forum?id=Zfx43ZZRZR>.

Li, S., Raghuram, V. C., Khattab, O., Hirschberg, J., and Yu, Z. Papillon: Privacy preservation from internet-based and local language model ensembles. In *North American Chapter of the Association for Computational Linguistics*, 2024. URL <https://api.semanticscholar.org/CorpusID:273507551>.

Li, S., Raghuram, V. C., Khattab, O., Hirschberg, J., and Yu, Z. PAPILLON: Privacy preservation from Internet-based and local language model ensembles. In Chiruzzo, L., Ritter, A., and Wang, L. (eds.), *Proceedings of the 2025 Conference of the Nations of the Americas Chapter of the Association for Computational Linguistics: Human Language Technologies (Volume 1: Long Papers)*, pp. 3371–3390, Albuquerque, New Mexico, April 2025. Association for Computational Linguistics. ISBN 979-8-89176-189-6. doi: 10.18653/v1/2025.nacl-long.173. URL [https://aclanthology.org/2025.nacl-long.173/](https://aclanthology.org/2025.nacl-long.173).

Lin, H., Wang, X., Yan, R., Huang, B., Ye, H., Zhu, J., Wang, Z., Zou, J., Ma, J., and Liang, Y. Generative evaluation of complex reasoning in large language models. *arXiv preprint arXiv:2504.02810*, 2025.

Meta AI. Introducing meta llama 3: The most capable openly available llm to date. <https://ai.meta.com/blog/meta-llama-3/>, April 2024. Accessed: 2025-09-24.

Muennighoff, N., Yang, Z., Shi, W., Li, X. L., Li, F.-F., Hajishirzi, H., Zettlemoyer, L. S., Liang, P., Candès, E. J., and Hashimoto, T. s1: Simple test-time scaling. *ArXiv*, abs/2501.19393, 2025. URL <https://api.semanticscholar.org/CorpusID:276079693>.

Ning, X., Lin, Z., Zhou, Z., Wang, Z., Yang, H., and Wang, Y. Skeleton-of-thought: Prompting LLMs for efficient parallel generation. In *The Twelfth International Conference on Learning Representations*, 2024. URL <https://openreview.net/forum?id=mcVgBbNCm9>.

OpenAI. Introducing gpt-5. <https://openai.com/index/introducing-gpt-5/>, August 2025. Accessed: 2025-09-24.

Qu, G., Chen, Q., Wei, W., Lin, Z., Chen, X., and Huang, K. Mobile edge intelligence for large language models: A contemporary survey. *IEEE Communications Surveys & Tutorials*, 2025.

Rein, D., Hou, B. L., Stickland, A. C., Petty, J., Pang, R. Y., Dirani, J., Michael, J., and Bowman, S. R. Gpqa: A graduate-level google-proof q&a benchmark. In *First Conference on Language Modeling*, 2024.

Shao, C., Hu, X., Lin, Y., and Xu, F. Division-of-thoughts: Harnessing hybrid language model synergy for efficient on-device agents. In *Proceedings of the ACM on Web Conference 2025*, pp. 1822–1833, 2025.

Tian, C., Qin, X., Tam, K., Li, L., Wang, Z., Zhao, Y., Zhang, M., and Xu, C. Clone: Customizing llms for efficient latency-aware inference at the edge. *arXiv preprint arXiv:2506.02847*, 2025.

Wang, F., Zhang, Z., Zhang, X., Wu, Z., Mo, T., Lu, Q., Wang, W., Li, R., Xu, J., Tang, X., et al. A comprehensive survey of small language models in the era of large language models: Techniques, enhancements, applications, collaboration with llms, and trustworthiness. *arXiv preprint arXiv:2411.03350*, 2024a.

Wang, S., Tan, Z., Chen, Z., Zhou, S., Chen, T., and Li, J. Anymac: Cascading flexible multi-agent collaboration via next-agent prediction. *arXiv preprint arXiv:2506.17784*, 2025.

Wang, Y., Ma, X., Zhang, G., Ni, Y., Chandra, A., Guo, S., Ren, W., Arulraj, A., He, X., Jiang, Z., et al. Mmlu-pro: A more robust and challenging multi-task language understanding benchmark. *arXiv preprint arXiv:2406.01574*, 2024b.

Wei, J., Wang, X., Schuurmans, D., Bosma, M., Xia, F., Chi, E., Le, Q. V., Zhou, D., et al. Chain-of-thought prompting elicits reasoning in large language models. *Advances in neural information processing systems*, 35:24824–24837, 2022.

White, C., Dooley, S., Roberts, M., Pal, A., Feuer, B., Jain, S., Shwartz-Ziv, R., Jain, N., Saifullah, K., Dey, S., Shubh-Agrawal, Sandha, S. S., Naidu, S. V., Hegde, C., LeCun, Y., Goldstein, T., Neiswanger, W., and Goldblum, M. Livebench: A challenging, contamination-limited LLM benchmark. In *The Thirteenth International Conference on Learning Representations*, 2025. URL <https://openreview.net/forum?id=sKYHBTaxVa>.

Xiong, S., Payani, A., Kompell, R., and Fekri, F. Large language models can learn temporal reasoning. In *Proceedings of the 62nd Annual Meeting of the Association for Computational Linguistics (Volume 1: Long Papers)*, pp. 10452–10470, 2024.

Yao, S., Yu, D., Zhao, J., Shafran, I., Griffiths, T., Cao, Y., and Narasimhan, K. Tree of thoughts: Deliberate problem solving with large language models. *Advances in neural information processing systems*, 36:11809–11822, 2023.

Ye, S., Ouyang, B., Zeng, L., Qian, T., Chu, X., Tang, J., and Chen, X. Jupiter: Fast and resource-efficient collaborative inference of generative llms on edge devices. In *IEEE INFOCOM 2025-IEEE Conference on Computer Communications*, pp. 1–10. IEEE, 2025.

Yu, Y., Zhang, Y., Zhang, D., Liang, X., Zhang, H., Zhang, X., Khademi, M., Awadalla, H. H., Wang, J., Yang, Y., and Wei, F. Chain-of-reasoning: Towards unified mathematical reasoning in large language models via a multi-paradigm perspective. In *Proceedings of the 63rd Annual Meeting of the Association for Computational Linguistics (Volume 1: Long Papers)*, pp. 24914–24937, July 2025.

Yuan, W., Neubig, G., and Liu, P. Bartscore: Evaluating generated text as text generation. *Advances in neural information processing systems*, 34:27263–27277, 2021.

Yuan, Z., Sun, W., Liu, Y., Zhou, H., Zhou, R., Li, Y., Zhang, Z., Song, W., Huang, Y., Jia, H., et al. Efficientllm: Efficiency in large language models. *arXiv preprint arXiv:2505.13840*, 2025.

Yue, M., Zhao, J., Zhang, M., Du, L., and Yao, Z. Large language model cascades with mixture of thoughts representations for cost-efficient reasoning. *arXiv preprint arXiv:2310.03094*, 2023.

Zhang, Y., Li, M., Long, D., Zhang, X., Lin, H., Yang, B., Xie, P., Yang, A., Liu, D., Lin, J., et al. Qwen3 embedding: Advancing text embedding and reranking through foundation models. *arXiv preprint arXiv:2506.05176*, 2025.

Zhou, C., Liu, P., Xu, P., Iyer, S., Sun, J., Mao, Y., Ma, X., Efrat, A., Yu, P., YU, L., Zhang, S., Ghosh, G., Lewis, M., Zettlemoyer, L., and Levy, O. LIMA: Less is more for alignment. In *Thirty-seventh Conference on Neural Information Processing Systems*, 2023. URL <https://openreview.net/forum?id=KBMOkmX2he>.

A. Notations

Table 4. Notations and definitions used in HybridFlow.

Notation	Definition
Q	User-issued query.
M_{edge}	Small edge model used for local inference.
M_{cloud}	Large cloud LLM accessed via API.
M_P	Edge-deployed planner model (Llama3.2–3B).
$T = \{t_i\}_{i=1}^n$	Set of subtasks produced from query Q .
E	Directed edge set encoding prerequisite relations between subtasks.
$G(Q) = (T, E)$	Task-level decomposition DAG for query Q .
n	Number of subtasks in the decomposition.
Δq_i	Expected accuracy gain of executing t_i on M_{cloud} vs. M_{edge} .
Δl_i	Additional latency cost (seconds) of executing t_i on M_{cloud} .
Δk_i	Additional API usage cost (tokens or price units) of executing t_i on M_{cloud} .
l_{\max}^{sub}	Per-subtask upper bound on additional latency for normalization.
k_{\max}^{sub}	Per-subtask upper bound on additional API cost for normalization.
c_i	Normalized cost of offloading t_i [Eq. (1)].
r_i	Routing decision for t_i : 1 if offloaded to M_{cloud} , 0 otherwise.
$\mathbf{r} = (r_1, \dots, r_n)$	Routing vector for all subtasks of a query.
C_{\max}	Total normalized resource budget for a query [Eq. (3)].
u_i	Utility (normalized benefit–cost ratio) of offloading t_i [Def. 3.2].
ε	Small positive constant (e.g., 10^{-4}) for numerical stability in u_i .
K_{\max}^{global}	Global API usage budget over the entire query.
L_{\max}^{global}	Global latency budget over the entire query.
k_{used}	Cumulative API usage consumed so far during inference.
l_{used}	Cumulative latency incurred so far during inference.
τ_0	Base routing threshold.
τ_t	Adaptive routing threshold at time t [Eq. (11)].
z_i	Semantic embedding of subtask t_i .
f_{θ}	Router network parameterized by θ .
\hat{u}_i	Predicted utility of offloading t_i .
$\sigma(\cdot)$	Sigmoid activation function used in the router.
$\mathcal{L}(\theta)$	Training loss for the router parameters θ .
N	Number of profiled subtasks used for router training.
\mathcal{Q}	Scheduler queue of <i>ready</i> subtasks in the DAG.

B. Optimization View of HybridFlow

This section provides a rigorous optimization formulation of the HybridFlow routing problem and establishes the theoretical underpinnings of the utility-based router introduced in Sec. 3.3. We formalize the allocation problem as a 0–1 knapsack problem, derive its Lagrangian relaxation, and show how the adaptive threshold mechanism used in HybridFlow naturally emerges as a primal–dual update for this relaxation.

B.1. 0–1 Knapsack Formulation

For a query decomposed into subtasks $T = \{t_1, \dots, t_n\}$, recall that Δq_i is the accuracy gain from offloading t_i to the cloud, $c_i \in [0, 1]$ is the normalized resource cost, and $r_i \in \{0, 1\}$ indicates whether t_i is offloaded. Let $C_{\max} \in [0, 1]$ denote the normalized per-query resource budget.

The routing problem in Sec. 3.3 can be written as:

$$\begin{aligned} \max_{\mathbf{r} \in \{0,1\}^n} \quad & \sum_{i=1}^n r_i \Delta q_i \\ \text{s.t.} \quad & \sum_{i=1}^n r_i c_i \leq C_{\max}, \end{aligned} \tag{15}$$

which is exactly the *0–1 knapsack problem*, with each subtask t_i corresponding to an item of value Δq_i and weight c_i . This formulation provides both: (i) a principled objective for allocation, and (ii) an optimal oracle via dynamic programming for evaluation.

B.2. Lagrangian Relaxation

We obtain a continuous relaxation of the knapsack by dualizing the budget constraint. Introducing a Lagrange multiplier $\lambda \geq 0$, the Lagrangian becomes:

$$\mathcal{L}(\mathbf{r}, \lambda) = \sum_{i=1}^n r_i \Delta q_i - \lambda \left(\sum_{i=1}^n r_i c_i - C_{\max} \right). \tag{16}$$

Expanding the expression yields:

$$\mathcal{L}(\mathbf{r}, \lambda) = \lambda C_{\max} + \sum_{i=1}^n r_i (\Delta q_i - \lambda c_i). \tag{17}$$

For a fixed λ , the optimization decomposes across subtasks:

$$r_i^*(\lambda) = \arg \max_{r_i \in \{0,1\}} r_i (\Delta q_i - \lambda c_i) = \mathbb{I}[\Delta q_i - \lambda c_i > 0], \tag{18}$$

where $\mathbb{I}[\cdot]$ is the indicator function.

Thus the relaxed problem prescribes the following thresholding rule:

$$\text{Offload } t_i \iff \frac{\Delta q_i}{c_i} > \lambda. \tag{19}$$

Here λ plays the role of a *shadow price* of resource consumption: subtasks with benefit–cost ratio above λ should be offloaded.

B.3. Primal–Dual Dynamics and Adaptive Thresholding

HybridFlow performs *online* allocation as subtasks become ready. A natural approach is to maintain a time-varying estimate of the shadow price λ_t and update it based on cumulative consumption. A standard primal–dual update for the constraint $\sum_i r_i c_i \leq C_{\max}$ is:

$$\lambda_{t+1} = [\lambda_t + \eta(C_{\text{used}} - C_{\max})]_+, \tag{20}$$

where $\eta > 0$ is a step size and $[\cdot]_+$ denotes projection onto $[0, \infty)$.

HybridFlow’s adaptive threshold in Eq. (11) of the main text,

$$\tau_t = \text{clip} \left(\tau_0 + \frac{k_{\text{used}}}{2K_{\max}^{\text{global}}} + \frac{l_{\text{used}}}{2L_{\max}^{\text{global}}}, 0, 1 \right), \tag{21}$$

is precisely an instance of a primal–dual update:

- the additive terms track *dual pressure* from API cost and latency,
- the clipping corresponds to projected dual ascent,

- the threshold τ_t plays the role of the shadow price λ_t in Eq. (19).

Thus HybridFlow’s routing rule,

$$\hat{u}_i > \tau_t \iff \frac{\Delta q_i}{c_i} \gtrsim \lambda_t, \quad (22)$$

is an online approximation to the Lagrangian decision rule in Eq. (18).

B.4. Learned Approximation to the Optimal Policy

HybridFlow does not observe Δq_i or c_i at inference time. Instead it uses learned utility estimates $\hat{u}_i \approx u_i$ obtained from a lightweight MLP. Under mild smoothness assumptions on the embedding mapping and the true utility function, the resulting allocation rule

$$r_i = \mathbb{I}[\hat{u}_i > \tau_t] \quad (23)$$

approximates the relaxed knapsack-optimal policy while ensuring online compliance with global resource budgets. The adaptive threshold thereby provides principled control over budget usage without requiring explicit dynamic programming.

B.5. Implications

This optimization analysis yields several insights:

- **Interpretability:** Each routing decision reduces to comparing a predicted marginal utility with a time-varying shadow price.
- **Optimality Structure:** The DP oracle defines an upper bound for achievable allocation quality; HybridFlow’s router approximates this solution in a computationally lightweight manner.
- **Budget Compliance:** The adaptive threshold implements a projected dual ascent rule, increasing conservativeness as resource usage grows.
- **Scalability:** Because the relaxed problem is decomposable, HybridFlow can make routing decisions independently across subtasks while preserving global budget coherence.

This provides a principled foundation for the design of HybridFlow’s routing mechanism and clarifies its connection to classical combinatorial optimization.

C. Implementation Details

Subtasks and decomposition DAG. Given an input query Q , HybridFlow represents a reasoning plan as a directed acyclic graph (DAG) $G(Q) = (T, E)$, where $T = \{t_1, \dots, t_n\}$ is the set of subtasks and $E \subseteq T \times T$ encodes prerequisite relations.

Definition C.1 (Subtask). A subtask is a tuple

$$t_i = (d_i, P_i, \tau_i),$$

where (i) d_i is a natural-language description of the operation to be performed (e.g., “Check whether the inverse property holds”), (ii) $P_i \subseteq \{1, \dots, n\} \setminus \{i\}$ is the index set of its prerequisite subtasks, and (iii) $\tau_i \in \{\text{EXPLAIN}, \text{ANALYZE}, \text{GENERATE}\}$ is a role label that follows the Explain–Analyze–Generate (EAG) metaprompt structure.

For convenience, we write $t_j \rightarrow t_i$ whenever $j \in P_i$. The edge set is then $E = \{(t_j, t_i) : j \in P_i, i = 1, \dots, n\}$.

Definition C.2 (Valid decomposition). A decomposition of Q is a DAG $G(Q) = (T, E)$ with $T = \{t_i\}_{i=1}^n$ that satisfies:

1. (Acyclicity) $G(Q)$ is acyclic.
2. (Rooted plan) There exists a unique root node t_{root} with $P_{\text{root}} = \emptyset$ and $\tau_{\text{root}} = \text{EXPLAIN}$.
3. (Reachability) Every subtask is reachable from the root: for all i , there exists a directed path $t_{\text{root}} \rightsquigarrow t_i$.

4. (Well-formed outputs) At least one node is labeled GENERATE, and every GENERATE node has no outgoing edges (i.e., it is a sink in $G(Q)$).

5. (Size constraint) The number of subtasks is bounded by a constant $n \leq n_{\max}$ (we use $n_{\max} = 7$ in experiments), which controls planner overhead.

We denote by $\mathcal{G}(Q)$ the set of all valid decompositions for query Q .

The planner M_P induces a (stochastic) mapping

$$\text{Decompose} : Q \mapsto G(Q) \in \mathcal{G}(Q),$$

implemented as a prompt-based generation of an XML-formatted plan followed by a deterministic parsing and validation procedure.

To train the proposed resource-aware router, we construct an offline profiling dataset from 3,000 sampled queries drawn from two benchmarks: MMLU-Pro (different from the main test samples) and Math500 (covering general knowledge reasoning, targeting structured, multi-step reasoning). For each query, we perform the complete pipeline of task decomposition, subtask allocation, and execution using both the edge and cloud models. During this process, we record the response quality, inference latency, and API cost for each subtask.

Quality and Cost Estimation. For every subtask t_i , we estimate the *accuracy gap* between the edge and cloud models using BartScore (Yuan et al., 2021), which provides a differentiable approximation of textual quality alignment. Let Δq_i denote the expected quality improvement when offloaded to the cloud, and $(\Delta l_i, \Delta k_i)$ represent the additional latency and API cost, respectively. We define the normalized cost term as:

$$c_i = \frac{1}{2} \cdot \frac{\Delta l_i}{10} + \frac{1}{2} \cdot \frac{\Delta k_i}{0.02}, \quad (24)$$

where the constants 10 and 0.02 correspond to the normalization scales of latency (seconds) and API cost (\$), ensuring $c_i \in [0, 1]$ across all profiled subtasks.

Training Objective. Each subtask is annotated with its measured $(\Delta q_i, \Delta l_i, \Delta k_i)$ values, and the corresponding target utility score is computed as:

$$s_i = \text{clip}\left(\frac{\Delta q_i}{c_i + \varepsilon}, 0, 1\right), \quad (25)$$

where ε prevents division by zero and s_i reflects the normalized benefit–cost ratio. The router model f_θ is trained to regress this target utility from the subtask embedding z_i via a mean-squared loss:

$$\mathcal{L}(\theta) = \frac{1}{N} \sum_{i=1}^N (f_\theta(z_i) - s_i)^2. \quad (26)$$

This offline training enables the router to approximate the benefit–cost trade-off without requiring online supervision during inference.

Adaptive Threshold Configuration. At inference time, the router compares its predicted utility \hat{s}_i against an adaptive threshold τ_t to decide whether to offload a subtask. The threshold evolves with real-time resource usage as:

$$\tau_t = \text{clip}\left(\tau_0 + \frac{k_{\text{used}}}{2K_{\max}} + \frac{l_{\text{used}}}{2L_{\max}}, 0, 1\right), \quad (27)$$

where k_{used} and l_{used} are the cumulative API and latency costs consumed so far. We empirically set $\tau_0 = 0.2$, $K_{\max} = 0.02$, and $L_{\max} = 20$ based on preliminary tuning across all benchmarks. This configuration ensures that the router starts with a balanced offloading policy and becomes progressively more conservative as resources are consumed, maintaining overall cost efficiency without degrading reasoning quality.

Table 5. Performance–cost trends under different fixed offload thresholds τ_0 on the GPQA benchmark.

Threshold	Offload Rate (%)	Accuracy (%)	Latency (s)	API Cost (\$)	Normalized Cost (↓)	Utility (↑)
1	0.00	25.54	11.99	0	N/A	N/A
0.9	15.51	35.51	13.89	0.0042	0.2000	0.4985
0.8	24.67	42.89	14.87	0.0059	0.2915	0.5952
0.7	28.85	44.51	15.02	0.0064	0.3115	0.6090
0.6	33.51	47.85	15.39	0.0073	0.3525	0.6329
0.5	41.18	51.62	15.88	0.0088	0.4145	0.6292
0.4	60.95	53.29	16.56	0.0105	0.4910	0.5652
0.3	66.51	54.13	17.87	0.0128	0.6140	0.4656
0.2	73.70	55.14	18.29	0.0144	0.6750	0.4385
0.1	82.84	55.41	18.35	0.0167	0.7355	0.4061
0	100.00	57.28	18.26	0.0185	0.7760	0.4090

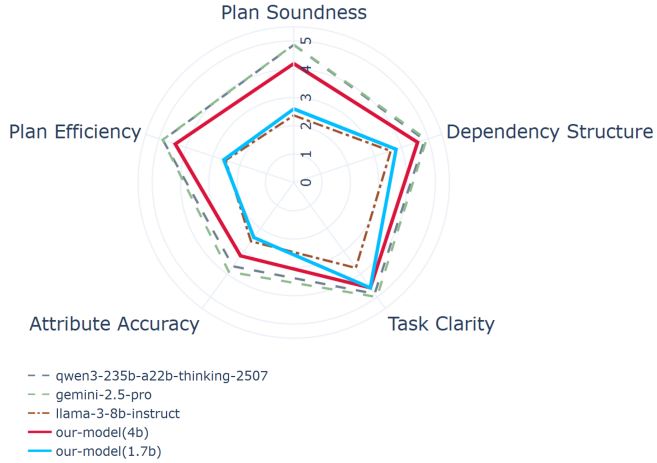


Figure 5. Results of our planner evaluation, assessing models on five key dimensions of task decomposition quality. We compare our two models (4B and 1.7B) against several leading standalone models, including Qwen3-235B-a22b-thinking-2507, Gemini-2.5-Pro, and Llama-3-8B-Instruct.

Summary. Through this profiling-based training and normalization procedure, the router learns a unified utility function that generalizes across different task domains and cost settings. It enables HybridFlow to make consistent, cost-aware routing decisions that align closely with the optimization objective in Eq. 3.

D. Supplementary Experiments

To formally assess the quality of a generated plan, we introduce a dual-faceted evaluation framework that moves beyond singular metrics like final task accuracy. A superior Planner’s quality is a function of both the intrinsic soundness of its generated plan and the extrinsic success of the Executor models in executing that plan. The absence of such a comprehensive metric in prior work makes objective comparison and targeted improvement of planning capabilities difficult. Our framework is designed to quantitatively measure these two facets, serving as the foundation for our subsequent data curation and model training efforts.

First, we assess the Intrinsic Plan Quality, which evaluates the machine-executable plan itself. This is judged across five key dimensions:

- **Plan Soundness & Decomposition:** This metric assesses whether the plan correctly and logically breaks down the problem. A flawed decomposition invalidates the entire solution strategy and is thus a primary point of evaluation.

- **Dependency Structure & Flow:** We evaluate the correctness of the task dependency graph. A logical dependency flow is crucial for maximizing parallelism and ensuring the correct context is passed between steps.
- **Task Clarity & Executability:** This dimension measures if each task is an unambiguous operational instruction suitable for an AI executor. Vague or poorly formulated tasks lead to poor downstream results.
- **Attribute Accuracy:** We judge the Planner’s estimation of Difficulty and Token attributes. Accurate estimations are vital for the efficient dynamic allocation of models by the Router.
- **Plan Relevance & Efficiency:** This checks for redundant or irrelevant steps. A high-quality plan must be lean, purposeful and free of wasted computations.

Second, we measure the Extrinsic Execution Performance, which evaluates the efficacy of the execution models when acting upon the instructions provided by the Planner. This directly links plan quality to downstream performance and is assessed on the following five dimensions:

- **Instruction Following & Adherence:** This metric assesses how well the Executor model adheres to the specific constraints and instructions of the assigned sub-task.
- **Effective Use of Context:** We evaluate whether the model correctly utilizes the provided results from prior, dependent steps to inform its own execution.
- **Correctness & Factual Accuracy:** This measures the factual and logical accuracy of the model’s response, serving as the primary measure of successful task completion.
- **Clarity & Machine Usability:** We judge whether the Executor’s output is clear, well-structured, and easily parsable for use in subsequent steps.
- **Relevance & Conciseness:** This assesses if the model’s response is concise and strictly relevant to the task, avoiding conversational filler or extraneous information.

Together, this dual-evaluation framework provides a comprehensive and structured methodology for analyzing both the plan and its real-world impact, enabling a systematic approach to enhancing the planning capabilities essential for effective hybrid model collaboration.

Recent advancements in enhancing Large Language Model (LLM) efficiency have increasingly focused on task decomposition. Prominent works such as SoT (Ning et al., 2024), DoT (Shao et al., 2025), and PASTA (Jin et al., 2025) exemplify this approach by leveraging parallel processing to improve time efficiency. However, these methods collectively raise two critical, unaddressed questions. First, **the field lacks a formal, quantitative methodology for measuring the intrinsic “quality” of the resulting plan itself**, making the comparison and optimization of planning capabilities difficult. Second, **it remains unknown whether this complex planning capability can be distilled from elite large models into a small model**.

We argue that addressing the second question is crucial for achieving efficient and scalable collaborative reasoning. If planning capabilities can be successfully distilled, a small model could undertake the core role of task decomposition. This would not only dramatically reduce latency and minimize API costs, yielding a cost-efficient, low-latency solution for complex reasoning, but it would also unlock new possibilities for edge deployment and even privacy-preserving scenarios (Li et al., 2024) where planning occurs locally. Therefore, the motivation for our work is twofold: first, through our Planner, we aim to establish a framework that can systematically evaluate plan quality; and second, we seek to demonstrate the feasibility of distilling this advanced capability from large to small models.

Distillation of Planning Capabilities Recent studies have demonstrated that substantial performance gains can be achieved by fine-tuning models on small, high-quality datasets (Zhou et al., 2023; Muennighoff et al., 2025). This paradigm raises a critical research question for our work: **Can the sophisticated planning capabilities inherent in elite large models be effectively distilled into a small model using a similarly curated, high-quality dataset?**

This question is motivated by a significant performance gap observed in our own benchmark results (Table 1). We found that the intrinsic planning ability of small models, such as Llama-3-8B (Meta AI, 2024), is substantially inferior to that of

state-of-the-art large models like GPT-5 (OpenAI, 2025). Bridging this gap is crucial for creating efficient and scalable collaborative systems.

To create this dataset, we developed a meticulous, benchmark-driven curation process. First, we used our Planner Evaluation Metric to identify top-performing LLMs. We then curated a set of “good” and “flawed” plan exemplars from their outputs to serve as didactic examples in a sophisticated meta-prompt. This prompt was used to guide a top-tier generative model to produce high-quality plans for the problems in the s1k dataset (Muennighoff et al., 2025).

We first evaluate the **effectiveness of the Planner**. This includes two aspects: the improvement in planning quality brought by Supervised Fine-Tuning (SFT), and the parallelization advantages introduced by task decomposition.

Table 6. Planner Performance Comparison
Worker: Llama3.2-3B, Dataset:GPQA

Planner	Avg. Steps	R_{comp}	C_{time}	Acc
Llama3.2-3B base	5.84	10.71	10.81	20.00
Llama3.2-3B SFT	6.12	34.3	11.59	22.00

Effectiveness of SFT: As shown in Table 6, our SFT Planner achieves an accuracy of 22.00% on GPQA, outperforming the planner based on the Llama3.2-3B base model (20.00% accuracy). This demonstrates the effectiveness of our distillation and fine-tuning process in generating high-quality, logically sound plans.

Parallelization Advantage: At the same time, Table 6 shows the SFT Planner achieves a 34.3% compression ratio. The compression ratio R_{comp} is defined as follows:

$$R_{comp} = (n - L_{crit})/n, \quad (28)$$

where n is the total number of steps and L_{crit} is the critical path length. This indicates that a significant number of steps within the tasks can be parallelized. HybridFlow’s DAG decomposition aims to strike a balance between two extremes: **fully sequential execution** ($R_{comp} = 0$) and **fully parallel execution** ($R_{comp} = (n - 1)/n$). Our method ensures accuracy by preserving critical dependencies while leveraging parallelization to significantly reduce end-to-end latency (C_{time}), making it faster than purely sequential execution.

D.1. Privacy Discussion: Data Exposure in Edge–Cloud Collaboration

HybridFlow is designed for efficient inference under resource budgets; it is not a privacy-preserving protocol and does not provide formal privacy guarantees. Here we give a concise analysis of *data exposure* to the cloud, i.e., what information is transmitted in API requests.

Threat model. We assume a standard cloud API setting where the cloud provider (or any entity with access to cloud logs) can observe the full content of each API request. We do not model a compromised device or side channels. The goal is to characterize and compare the amount of transmitted information across paradigms.

Transmitted content under different paradigms. Let Q denote the original user query. HybridFlow decomposes Q into subtasks organized as a DAG. For a subtask s_i , let $\text{Dep}(i)$ be its prerequisite subtasks and let a_j be the generated answer for s_j . When HybridFlow offloads s_i to the cloud, the transmitted payload contains:

$$x_i \triangleq (s_i, \{a_j\}_{j \in \text{Dep}(i)}), \quad (29)$$

i.e., the current subtask and the answers of its dependencies, **without transmitting the original query Q** . In contrast, cloud-only inference transmits the full Q (often along with additional prompts/history), while edge-only inference transmits nothing to the cloud.

Exposure proxy. To quantify cloud exposure in a model-agnostic way, we define a token-based proxy:

$$E_{\text{cloud}} \triangleq \sum_{i \in \mathcal{C}} \text{tok}(x_i), \quad (30)$$

Method	Accuracy	API Cost ($\times 10^{-3}$ \$)	Latency (s)
All-Edge CoT (Qwen2.5-7B)	34%	NA	19.52
All-Cloud CoT (DeepSeek-V3)	59%	6.70	61.00
HybridLLM (Ding et al., 2024)	47%	3.63	47.87
DoT (Shao et al., 2025)	49%	1.80	40.90
HybridFlow (Ours)	53%	1.16	36.86

Table 7. GPQA results under a swapped edge/cloud model pair (Qwen2.5-7B on edge; DeepSeek-V3 on cloud), with all other pipeline configurations unchanged. API cost is reported only for methods that invoke cloud APIs.

where \mathcal{C} is the set of subtasks routed to the cloud and $\text{tok}(\cdot)$ counts the number of tokens in the transmitted API payload.¹ We also report a normalized proxy

$$\bar{E}_{\text{cloud}} \triangleq \frac{E_{\text{cloud}}}{\sum_{i \in \mathcal{E}} \text{tok}(x_i) + \sum_{i \in \mathcal{C}} \text{tok}(x_i)}, \quad (31)$$

where \mathcal{E} is the set of subtasks executed on the edge. This normalization reflects the fraction of total subtask-level information that is transmitted to the cloud.

Implications and limitations. HybridFlow can reduce exposure relative to cloud-only inference because it (i) offloads only a subset of subtasks and (ii) transmits only $(s_i, \{a_j\}_{j \in \text{Dep}(i)})$ rather than the full Q . However, exposure is not eliminated: if sensitive information is required to solve an offloaded subtask or is present in dependency answers $\{a_j\}$, it will be included in x_i and observed by the cloud. More broadly, HybridFlow should be viewed as reducing the *surface area* of cloud-visible content in favorable cases, rather than guaranteeing privacy.

D.2. Model-Pair Swap: Generality Across Edge/Cloud Models

Our main experiments instantiate the edge–cloud pipeline with **Llama3.2-3B** (edge) and **GPT-4.1** (cloud). To test whether HybridFlow depends on a particular model pair, we conduct a *model-pair swap* on GPQA: we replace the edge model with **Qwen2.5-7B** and the cloud model with **DeepSeek-V3**, while keeping the rest of the system *unchanged* (task decomposition and prompting format, routing/scheduling logic, budget settings, and the evaluation protocol). All edge–cloud baselines are evaluated under the same swapped model pair for a fair comparison. Results are shown in Table 7.

Discussion. The swapped pair exhibits the expected edge/cloud extremes: All-Edge is fast (19.52s) but less accurate (34%), whereas All-Cloud is more accurate (59%) but substantially more expensive and slower (6.70×10^{-3} \$, 61.00s). Under the same swapped pair, HybridFlow maintains a strong cost–latency–accuracy trade-off against edge–cloud baselines: compared to DoT, HybridFlow improves accuracy by 4 points (49%→53%) while reducing API cost by 35.6% (1.80→1.16) and latency by 9.9% (40.90s→36.86s); compared to HybridLLM, it improves accuracy by 6 points and reduces API cost and latency by 68.0% and 23.0%, respectively. Overall, this model-pair swap suggests HybridFlow’s subtask-level routing and dependency-aware scheduling are not specialized to the Llama3.2-3B/GPT-4.1 instantiation, and can transfer to a different edge/cloud model pair with minimal changes. We view this as evidence of transfer across model scales, while broader coverage of model families is left for future work.

¹If desired, one can include the cloud-generated output tokens as well by adding $\sum_{i \in \mathcal{C}} \text{tok}(y_i)$, where y_i is the cloud response. We focus on transmitted inputs since they directly encode user-provided and intermediate information.

You are a precise planning agent. Decompose the user's task into a sequence of concrete, easy-to-solve sub_problems. Use high-level EAG-style roles implicitly (Explain → Analyze → Generate), but keep each sub_problem as a single sentence question.

Plan Structure: EAG framework

- **Explain:** To assist the following agents, what is your understanding of the question after reviewing it, focusing only on essential information and filtering out all irrelevant details
- **Analyze:** Break down the problem into the smallest possible, independent sub_tasks to solve the problem. These steps should rely on the "Explain" step or other completed analysis steps.
- **Generate:** After reviewing the original question and the thoughts of previous agents, generate the final answer to the question.

XML Plan Constraints:

- **id:** A unique integer (must be < 7 steps)
- **desc:** The question for executor AI
- **depends_on:** ID(s) of prerequisite steps (comma-separated if multiple)

Return ONLY the XML plan as final output. No additional text.

Examples:

```
<Plan>      <Step ID="1" Task="Explain: What is the set (real numbers) and the
operation (multiplication) in question, and what is the core assertion (that it's
not a group) that needs to be verified?" Rely="" />      <Step ID="2" Task="Analyze:
Check the closure property: Is multiplication a binary operation on the set of
all real numbers?" Rely="1" />      <Step ID="3" Task="Analyze: Check the associative
property: Is multiplication of real numbers associative?" Rely="1" />      <Step ID="4"
Task="Analyze: Check the identity property: Is there an identity element for
multiplication in the set of real numbers?" Rely="1" />      <Step ID="5" Task="Analyze:
Check the inverse property: Does every element in the set of real numbers have a
multiplicative inverse?" Rely="1" />      <Step ID="6" Task="Generate: After reviewing
the original question and the thoughts of previous agents, what is the final
answer to the question?" Rely="2,3,4,5" /></Plan>

<Plan>  <Step ID="1" Task="Explain: What is the base field, what are the adjoined
elements (sqrt(2), sqrt(3), sqrt(18)), and what is the required final output
format?" Rely="" />  <Step ID="2" Task="Analyze: What is the minimal polynomial
for sqrt(2) over Q, and what is the degree [Q(sqrt(2)) : Q]?" Rely="1" />  ...
(truncated for brevity) ... <Step ID="8" Task="Generate: Based on the final degree
calculated in Step 7, what is the correct option letter and its corresponding
content?" Rely="1,7" /></Plan>

<Plan>  <Step ID="1" Task="Explain: What is the set (real numbers), the operation
(multiplication), and the required output (option letter and content)?" Rely="" />
... (truncated for brevity) ... <Step ID="6" Task="Generate: Based on the
analysis of the group axioms in steps 2-5, which option correctly identifies
the reason this is not a group, and what is the final option letter and content?" Rely="2,3,4,5" /></Plan>
```

Now is your turn:

Figure 6. Planner prompt for task decomposition.

Original Question:

"Given a reaction starting with 4,5-dimethylcyclohex-4-ene-1,2-dicarbonitrile and forming 2,3-dimethylbuta-1,3-diene and maleonitrile. Explain why adding maleic anhydride causes the reaction to shift more to the right.
A. Maleic anhydride converts into 4,5-dimethylcyclohex-4-ene-1,2-dicarbonitrile and this causes the equilibrium to shift towards reactants.
B. Maleic anhydride reacts with 4,5-dimethylcyclohex-4-ene-1,2-dicarbonitrile and addition of a reactant causes the equilibrium to shift towards products.
C. Maleic anhydride reacts with 2,3-dimethylbuta-1,3-diene and removal of a product causes the equilibrium to shift towards products.
D. Maleic anhydride converts into maleonitrile and addition of a product causes the equilibrium to shift towards products."

Task Decomposition and Execution:

```
"subtasks": [{  
  "id": "1",  
  "desc": "Explain: list the reactants, products, and the effect of adding maleic anhydride on the reaction.",  
  "depends_on": [],  
  "model_type": "cloud",  
  "answer": "Reactants: 4,5-dimethylcyclohex-4-ene-1,2-dicarbonitrile \nProducts: 2,3-dimethylbuta-1,3-diene and maleonitrile \nEffect of adding maleic anhydride: It reacts with one of the products, removing it from the equilibrium and shifting the reaction towards the products side."  
, {  
  "id": "2",  
  "desc": "Analyze: describe the reaction mechanism and equilibrium shift caused by maleic anhydride.",  
  "depends_on": ["1"],  
  "model_type": "edge",  
  "answer": "Sub-problem 2 answer: \nMaleic anhydride reacts with 2,3-dimethylbuta-1,3-diene, forming maleonitrile and a dienol. The removal of maleonitrile from the equilibrium causes the reaction to shift more towards the product 2,3-dimethylbuta-1,3-diene, resulting in an increased yield of the desired product."  
, {  
  "id": "3",  
  "desc": "Analyze: evaluate the effect of maleic anhydride conversion to maleonitrile on the reaction equilibrium.",  
  "depends_on": ["1", "2"],  
  "model_type": "cloud",  
  "answer": "The conversion of maleic anhydride to maleonitrile effectively removes maleonitrile, a product of the original reaction, from the equilibrium mixture. According to Le Chatelier's principle, removing a product shifts the equilibrium towards the products side to compensate. Therefore, this conversion drives the reaction forward, increasing the formation of 2,3-dimethylbuta-1,3-diene and maleonitrile.\n\nFinal answer: C. Maleic anhydride reacts with 2,3-dimethylbuta-1,3-diene and removal of a product causes the equilibrium to shift towards products."  
, {  
  "id": "4",  
  "desc": "Generate: select the correct answer based on the analysis.",  
  "depends_on": ["1", "2", "3"],  
  "model_type": "edge",  
  "answer": "Based on the analysis, the correct answer is:\n\nC. Maleic anhydride reacts with 2,3-dimethylbuta-1,3-diene and removal of a product causes the equilibrium to shift towards products.\n\nThis is because maleic anhydride reacts with 2,3-dimethylbuta-1,3-diene to form maleonitrile and a dienol, and the removal of maleonitrile from the equilibrium causes the reaction to shift more towards the product 2,3-dimethylbuta-1,3-diene."  
}]
```

Final Answer:

"C. Maleic anhydride reacts with 2,3-dimethylbuta-1,3-diene and removal of a product causes the equilibrium to shift towards products."

Figure 7. HybridFlow case study.